



Contents lists available at ScienceDirect

International Biodeterioration & Biodegradation

journal homepage: www.elsevier.com/locate/ibiod

Correlation between triphenyltin degradation and cellular metabolic responses of *Bacillus thuringiensis*



Wenying Yi, Chongshu Li, Jinshao Ye*, Yan Long, Huaming Qin

School of Environment, Jinan University, Guangzhou 510632, China

ARTICLE INFO

Article history:

Received 26 August 2016

Received in revised form

20 April 2017

Accepted 22 April 2017

Available online 28 April 2017

Keywords:

Degradation

Sorption

Triphenyltin

Organotin

Bacillus thuringiensis

ABSTRACT

The widespread use of triphenyltin, one of several organometallic endocrine disruptors, is leading to pollution of the natural environment. However, limited information is available about the dephenylation pathway and cellular responses that occur during the triphenyltin biodegradation process. Therefore, triphenyltin biosorption and degradation by *Bacillus thuringiensis* as well as its ion metabolism, nutrient use, membrane permeability, cellular morphology and ATPase activities were investigated using gas chromatography–mass spectrometry, ion chromatography and scanning electronic microscopy. The results revealed that triphenyltin was successively transformed to diphenyltin, monophenyltin and tin. The degradation and removal efficiencies of triphenyltin at 1 mg L⁻¹ by 0.3 g L⁻¹ of viable cells at 7 d were 78.2% and 95.3%, respectively, whereas the adsorption efficiency by inactivated cells was 63.3%. During this process, arabinose, oxalic acid, Na⁺, NH₄⁺, Mg²⁺, NO₃⁻, endospores and crystalline proteins were released. Based on computational analysis, it was inferred that triphenyltin was easily absorbed by teichoic acids in the cell wall, which altered the topological structure of peptidoglycans and the membrane. The increased assimilation of K⁺ and PO₄³⁻, reuse of released materials, and up-regulated expression of Na⁺/K⁺- and Ca²⁺/Mg²⁺-ATPases improved cellular viability, enhanced metabolic use of carbon, and increased phenyltin sorption and degradation.

© 2017 Elsevier Ltd. All rights reserved.

1. Introduction

Organotins (OTs) are organometallic compounds that are widely used as biocides, catalysts, antifouling agents, wood and textile preservatives, and plastic stabilizers (Adams et al., 2011; Fortibuoni et al., 2013). Among the most hazardous pollutants released into ecosystems, OT toxicity is directly related to the number of organic moieties and their properties (Oliveira and Santelli, 2010). Triphenyltin (TPT) is a highly substituted OT whose widespread use is polluting the global ecosystem.

To convert this endocrine disruptor into less toxic or non-toxic compounds, direct photolysis (Zhao et al., 2011), chemical cleavage and biological transformation (Gao et al., 2014) were investigated. The results revealed that biological methods were able to effectively eliminate TPT. In efforts to determine optimal conditions, appropriate concentrations of some additional surfactants and nutrients were used and found to enhance the degradation efficiency (Mathurasa et al., 2012; Tang et al., 2016). TPT transport

and transformation by effective microbes are metabolically mediated activities (Lu et al., 2017). To delineate the mechanisms involved, including surface binding, transport, intracellular transformation and accumulation, it is vital to study the cellular responses during this process.

Of these activities, TPT biosorption and transport are the initial and important reactions and have been confirmed through TPT binding by *Stenotrophomonas maltophilia* (Gao et al., 2014) and TPT biosorption by *Brevibacillus brevis* (Ye et al., 2013a). The components of the bacterial peptidoglycan layers play a key role in TPT binding, uptake and transformation (Tang et al., 2016). To enhance TPT biodegradation and delineate the mechanisms underlying TPT biosorption and transport, it is critically important to determine the relationship between the pollutant's molecular properties and those of the cell wall and membrane.

With regard to the intracellular transformation pathway, it was inferred from the detected intermediates that TPT was successively dearylated, producing diphenyltin (DPT), monophenyltin (MPT) and tin (Yi et al., 2012). The TPT → DPT → MPT transformation was recognized as a fast process, in contrast to MPT dearylation (Huang et al., 2014). However, direct degradation of trisubstituted species

* Corresponding author.

E-mail address: jsye@jnu.edu.cn (J. Ye).

to monosubstituted metabolites was scarcely observed. Given that in the TPT structure, three benzene rings are separately linked to tin, cleavage of these tin-carbon bonds might occur sequentially or synchronously. Therefore, investigating the dearylation pattern is vital for clarifying the TPT degradation mechanism.

Bacillus thuringiensis is a widespread bacterium that forms endospores, which ensures the resistance of this species to a variety of stresses, including exposure to pollutants (Renzi et al., 2016). Efficient degradation of some toxic xenobiotics, such as dimethyl phthalate (Surhio et al., 2014) and fipronil (Mandal et al., 2013), by some *B. thuringiensis* strains has been demonstrated. To examine the potential of this species to degrade emerging contaminants, such as phenyltins (PTs), an effective *B. thuringiensis* strain separated from OT contaminated sediments was used to decompose TPT in the present study. The TPT sorption, transport and biodegradation pathways, as well as microbial responses, such as cellular viability, morphological changes, membrane permeability, ion metabolism, protein expression, ATPase activity and nutrient use during these processes, were examined.

2. Materials and methods

2.1. Strain and chemicals

B. thuringiensis was isolated from OT contaminated sediment samples collected from Guiyu in Guangdong Province, China. The sequence of 16s RNA was analyzed and submitted to GenBank under accession number KY753445. Triphenyltin chloride was obtained from Sigma-Aldrich (St. Louis, MO, USA). The beef extract medium (BEM) used for bacterial culture contained 5 g L⁻¹ beef extract, 10 g L⁻¹ peptone, 1 g L⁻¹ NaCl and 10 mg L⁻¹ MgSO₄ with a pH of 7.2–7.4. Mineral salt medium (MSM) for TPT degradation consisted of (in mg L⁻¹) 50 KH₂PO₄, 50 NaCl, 30 NH₄Cl, 20 NH₄NO₃, 2 ZnSO₄·7H₂O, 2 MgSO₄ and 2 CaCl₂.

2.2. Biodegradation experiments

B. thuringiensis was cultured in BEM at 37 °C in a Petri dish for 1 d. Subsequently, the cells were harvested and used to degrade TPT. Flasks with 20 mL of MSM containing 1 mg L⁻¹ TPT and 0.3 g L⁻¹ *B. thuringiensis* were shaken in the dark at 25 °C for 0.5–7 d at 100 r min⁻¹. Subsequently, the cells were separated by centrifugation at 3500g for 10 min. Residual TPT in the supernatant was detected to determine the amount to be removed, and the total residual TPT in the supernatant and cells was used to determine biodegradation efficiency. The concentrations of Cl⁻, PO₄³⁻, Na⁺, NH₄⁺, K⁺, Mg²⁺ and extracellular protein in MSM, as well as intracellular protein, were determined to understand the correlation between TPT degradation and cellular metabolism. The effect of 1 mg L⁻¹ glucose on cellular responses was compared with that of TPT stress. The controls were run in parallel in flasks with MSM that were not inoculated. The mean values of three parallel samples for each experiment were used in the calculations.

2.3. TPT sorption and desorption by inactivated cells

To delineate the contribution of metabolism-independent sorption to TPT removal, biosorption was performed with cells inactivated by 2.5% glutaraldehyde for 1 d. Flasks with 20 mL of MSM containing 1 mg L⁻¹ TPT and 0.3 g L⁻¹ inactivated *B. thuringiensis* were shaken in the dark at 25 °C at 100 r min⁻¹ for 0.5–7 d. After cell separation, the residual TPT in the supernatant was analyzed to determine sorption efficiency. To examine TPT desorption, TPT-loaded cells were washed twice with phosphate buffer solution (PBS) for 30 min, and the desorbed TPT was

quantified.

2.4. Extraction and analysis of PTs

Extraction, derivatization and analysis of PTs were performed according to previously published methods (Ye et al., 2013a). Briefly, the PTs were analyzed by gas chromatography–mass spectrometry (GC–MS) (QP2010, Shimadzu, Japan) equipped with an Rxi-5MS GC column (30 m × 0.25 mm × 0.25 μm). Helium was used as the carrier gas with a constant flow of 1.1 mL min⁻¹. The column temperature program started at 50 °C and was held for 1.5 min. Subsequently, the oven was heated to 300 °C at a rate of 10 °C min⁻¹ and held for 4 min. The solvent cut time was set to 2.6 min. The GC–MS interface temperature was maintained at 280 °C. Mass spectra were recorded at 1 scan s⁻¹ under electronic impact with electron energy of 70 eV and a mass range of 50–650 atoms to mass unit. The temperature of the ion source was set at 250 °C. The sample (2 μL) was injected directly. The detection limits of TPT, DPT and MPT were 250, 110 and 110 ng L⁻¹, respectively.

2.5. Analysis of ions in MSM

After TPT degradation, the MSM was centrifuged at 3500 g for 10 min. The concentrations of Cl⁻, NO₃⁻, PO₄³⁻, Na⁺, NH₄⁺, K⁺ and Mg²⁺ in the supernatant were detected by an ICS-900 Ion Chromatography System (Dionex, Sunnyvale, USA) (Ye et al., 2013b).

2.6. Determination of membrane permeability and cellular morphology

o-Nitrophenyl-β-D-galactoside (ONPG) was used as the substrate to determine membrane permeability by measuring the concentration of β-galactosidase released into the MSM (Shi et al., 2013). Briefly, cells inoculated in BEM for 24 h were collected, washed and suspended in 0.9% NaCl solution. The suspension was added into lactose induction medium (in g L⁻¹: KH₂PO₄ 3, Na₂HPO₄·7H₂O 12.8, NaCl 0.5, NH₄Cl 1, MgSO₄ 0.5, CaCl₂ 0.01, lactose 5) and incubated at 37 °C. Subsequently, cells were collected, washed and suspended in β-galactosidase buffer (in g L⁻¹: KH₂PO₄ 0.24, Na₂HPO₄·12H₂O 2.9, NaCl 8, KCl 0.2, MgSO₄·7H₂O 0.25, β-mercaptoethanol 3.9 mL). Next, cells were treated with 1 mg L⁻¹ TPT in the presence of 1 g L⁻¹ ONPG. The production of o-nitrophenol was detected at 504 nm.

The surface morphology of the cells and crystalline proteins was observed using a scanning electronic microscope (SEM) (Philips XL-30E). Briefly, samples were fixed using glutaraldehyde for 24 h. Next, ethanol at 20%, 50%, 70% and 100% was used for cell dehydration. Subsequently, samples were immersed in isoamyl acetate for 30 min before a 4-h drying process at the breakthrough point using CO₂ as the refrigerant. After coating with gold in vacuum to improve conductivity, the samples were observed and photographed by SEM.

2.7. Analysis of total protein concentration and ATPase activities

After TPT degradation, the cells were separated, washed three times in cold PBS (pH 7.4), suspended in cold lysis buffer (30 mM Tris-HCl, 7 M urea, 2 M thiourea, and 4% w/v CHAPS at pH 8.5), and lysed by sonication in an ice bath for 15 min. The cellular debris was removed from the suspension by centrifugation at 16,000g for 5 min at 4 °C. The supernatant protein concentration was quantified by the Bradford method. Na⁺/K⁺- and Ca²⁺/Mg²⁺-ATPase activities were analyzed according to the instructions provided in the test kit, which was obtained from Nanjing Jiancheng Bioengineering Institute, China.

2.8. Metabolic use of carbon nutrients after TPT degradation

After TPT degradation, 1 mL of MSM was diluted in 99 mL of 0.85% sterilized NaCl solution. Next, 150 μ L of the sample was added to each well of a Biolog microplate and incubated at 25 °C in the dark. The optical density (OD_{590}) of each well was detected every 12 h. Cellular use of nutrients was analyzed by an average of the OD_{590} for each nutrient.

2.9. Computational methods

The structures of TPT, peptidoglycan and the cell membrane were drawn using ChemBioDraw Ultra version 13.0 and then copied to ChemBio3D Ultra version 13.0 to create three-dimensional models. Subsequently, these structures were subjected to energy minimization by molecular mechanics until the root-mean-square gradient became smaller than 0.01 kcal mol⁻¹ Å⁻¹. The interactions between TPT and the cellular components were analyzed using molecular dynamics. The step interval, frame interval and terminate of the calculation were 2 fs, 10 fs and 10,000 steps, respectively. The bond atom, dihedral atom and angle atom characteristics of the interacting molecules were computed.

2.10. Bioinformatics analysis of proteins related to material transport

The proteome of *B. thuringiensis* was searched and downloaded from the Universal Protein Resource database (UniProt) (<http://www.uniprot.org>). To select and identify the target proteins related to the transport of intracellular materials, functional analyses of the proteome were performed by using the String database (<http://string-db.org/>), Panther database (<http://www.pantherdb.org/>) and DAVID software version 6.8 (<http://david.abcc.ncifcrf.gov>).

3. Results

3.1. TPT sorption and degradation

TPT removal exhibited a slowly descending trend from 0.5 to 1 d followed by an ascending tendency from 72.6% to 95.3% at 0.5–7 d (Fig. 1A). Meanwhile, a rapidly increasing trend of TPT degradation from 1 to 2 d was followed by a slowly decreasing period with a degradation efficiency of up to 78.2% (Fig. 1A). TPT sorption by the cell surface showed a descending trend from 81% at 0.5 d to 63.3% at 7 d (Fig. 1B). The sorption reached its summit value of 81% at 0.5 d (Fig. 1B), which indicated that TPT binding was a rapid process associated with the hydrophobic interaction between TPT, and the cell wall and cell membrane. TPT desorption was partially responsible for the declining TPT sorption by inactivated cells (Fig. 1B) and the slow increase in TPT removal by viable cells over time (Fig. 1A).

3.2. The interaction between TPT and cellular components

As the transition states and intermediate structures formed by the binding of the cell wall to the pollutants during the biosorption process have short lifetimes, they are hard to analyze experimentally (Wang et al., 2015). To further understand TPT biosorption, the interaction between TPT and the cell wall was analyzed *in silico* using ChemBio3D Ultra 13.0. Fig. 2A shows that the –C–C–C–C–chain of the teichoic acids of peptidoglycans in the cell wall displayed intense affinity for TPT, which could alter the topological structure of the peptide chains, forming pores 12–15 Å in diameter in the peptidoglycan layer (Fig. 2A). Therefore, TPT is easily absorbed and transported into the cell wall (Fig. 2B) given that its

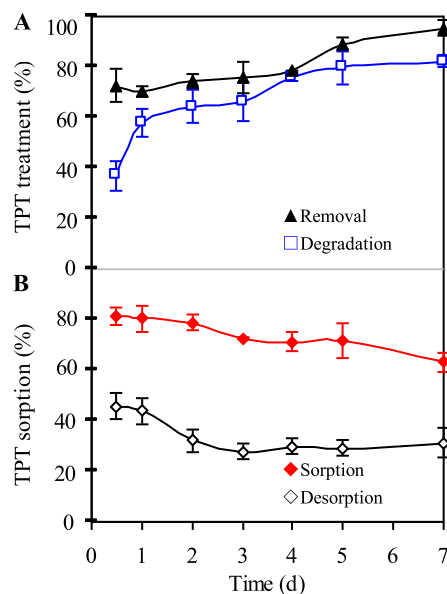


Fig. 1. Treatment of 1 mg L⁻¹ TPT by 0.3 g L⁻¹ *B. thuringiensis* for 0.5–7 d at 25 °C. (A) Degradation and removal of TPT by viable cells, (B) sorption and desorption of TPT by inactivated cells.

diameter is less than 11 Å. Fig. 2C confirms that some amount of TPT in the cell wall was desorbed as the concentration of the absorbed TPT increased due to repulsion among TPT molecules, whereas some TPT diffused into the periplasmic space for transport across the cell membrane.

3.3. Membrane permeability, arabinose and oxalic acid release during TPT biodegradation

The exposure of *B. thuringiensis* to TPT altered cellular membrane permeability (Fig. 3A), which was confirmed by computational analysis. The hydrophobic tails of the phospholipids with 14–22 carbons (Deleu et al., 2014) exhibited intense affinity for PTs (Fig. S1). Cellular viability, shown in Fig. 3A, established that some cells were dead at the experimental intervals. The released intracellular materials were assimilated by the viable cells. The decreasing toxicity of residual TPT also contributed to viability. In the current experiments, arabinose and oxalic acid were not added externally; therefore, their presence in MSM can be attributed to cellular release. Fig. 3B shows that their efflux consisted of an initial rapidly increasing phase and a subsequent decreasing phase. Fig. 3C shows that in comparison to TPT stress, glucose noticeably decreased the release of arabinose and oxalic acid.

3.4. Cellular morphology

As shown in Fig. 4, the exposure to TPT had a detrimental effect on *B. thuringiensis* and induced the death of some cells, releasing their endospores and crystalline proteins (Fig. 4A and B). However, the morphology of viable cells did not show visible differences compared with the control ones (Fig. 4C).

3.5. Ion metabolism and ATPase activities during TPT biodegradation

A negative value of ion concentration shown in Fig. 5 represents ion assimilation, and a positive one stands for ion release. Na⁺, NH₄⁺, Mg²⁺ and NO₃⁻ were released, whereas K⁺ and PO₄³⁻ were

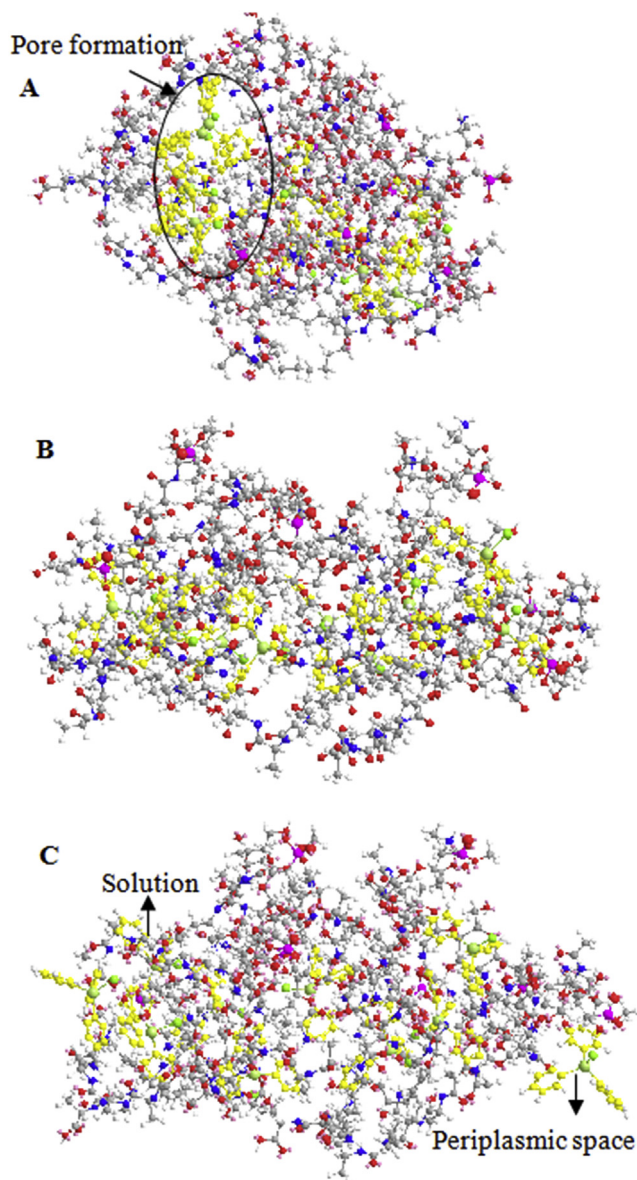


Fig. 2. The interaction between TPT and cellular components. (A) Pore formation of cell, (B) TPT transported into the cell wall, (C) a portion of TPT in the cell wall.

assimilated. Cl^- varied between uptake and release during TPT treatment (Fig. 5A and C). In contrast to TPT stress, glucose significantly decreased Na^+ release, increased PO_4^{3-} and Cl^- assimilation, and shifted Mg^{2+} and NH_4^+ release to uptake (Fig. 5B and D). These findings clearly confirmed that exposure to TPT was responsible for the increased release of ions and other materials.

The rapid increase in Na^+/K^+ - and $\text{Ca}^{2+}/\text{Mg}^{2+}$ -ATPase activities in the first period (Fig. 5E) were consistent with the trend for TPT degradation (Fig. 1A). The subsequent decrease in activity was partially responsible for the slowly increasing phase of TPT degradation. These findings demonstrated that these enzymes participated in TPT degradation.

3.6. Analysis of ion transport proteins

Based on the bioinformatics analysis, 18 ion transport proteins were identified (Table S1), which were related to potassium, sodium, magnesium, ammonium, phosphate and nitrate transport,

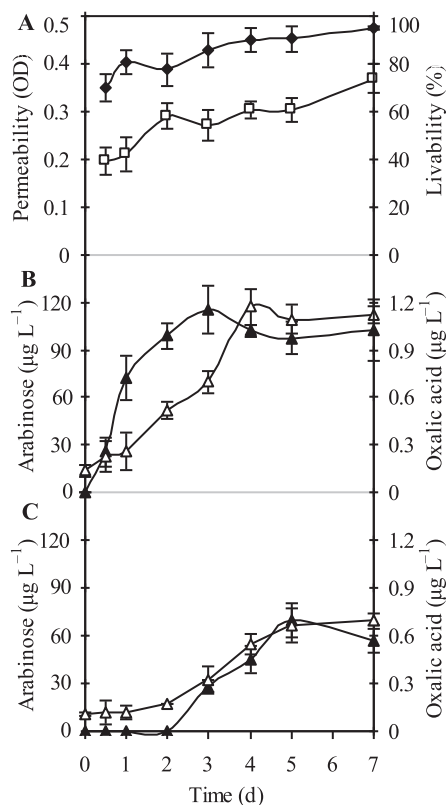


Fig. 3. Intracellular material release during the degradation of 1 mg L^{-1} TPT by 0.3 g L^{-1} *B. thuringiensis*. (A) Cellular viability and membrane permeability, (B) arabinose and oxalic acid release, (C) arabinose and oxalic acid release in the presence of 1 mg L^{-1} glucose without TPT.

respectively.

3.7. Metabolic use of nutrients after TPT degradation

Although the Biolog ECO plates contained 31 species of carbon, only 8 types were principal components that account for metabolic use of nutrients. Fig. S2 shows that *B. thuringiensis* preferred assimilating amino acids, carboxylic acids and polymers, rather than amines, carbohydrates and aromatic compounds. The substrate metabolic pattern of this strain shared similarities in carbon use with other microbial communities because amino acids and carboxylic acids are the most easily assimilated nutrients (Takabe et al., 2014). The lower assimilation of carbohydrates was consistent with arabinose release as shown in Fig. 3B. After TPT degradation, L-asparagine, D-malic acid, D-glucosaminic acid and glycyl-L-glutamic acid use was significantly increased, whereas L-threonine and pyruvic acid methyl ester assimilation decreased. The transport of Tween 40 and 4-hydroxy-benzoic acid did not exhibit significant differences in comparison with the control. Microbes possess some resistance mechanisms to pollutants, such as the superoxide dismutases and the metallothioneins (Schmidt et al., 2009). However, *B. thuringiensis* tended to form spores to resist PTs. During this process, abundant oligopeptides and amino acids are required, which enhanced the assimilation of extracellular amino acids (Renzi et al., 2016). Although TPT is an enzyme inhibitor, the increased OD_{590} of the Biolog plate revealed that the prohibitive effects of TPT stress on metabolic activity were lower than that of nutrient deficiency in the control, which had no external source of organic carbon.

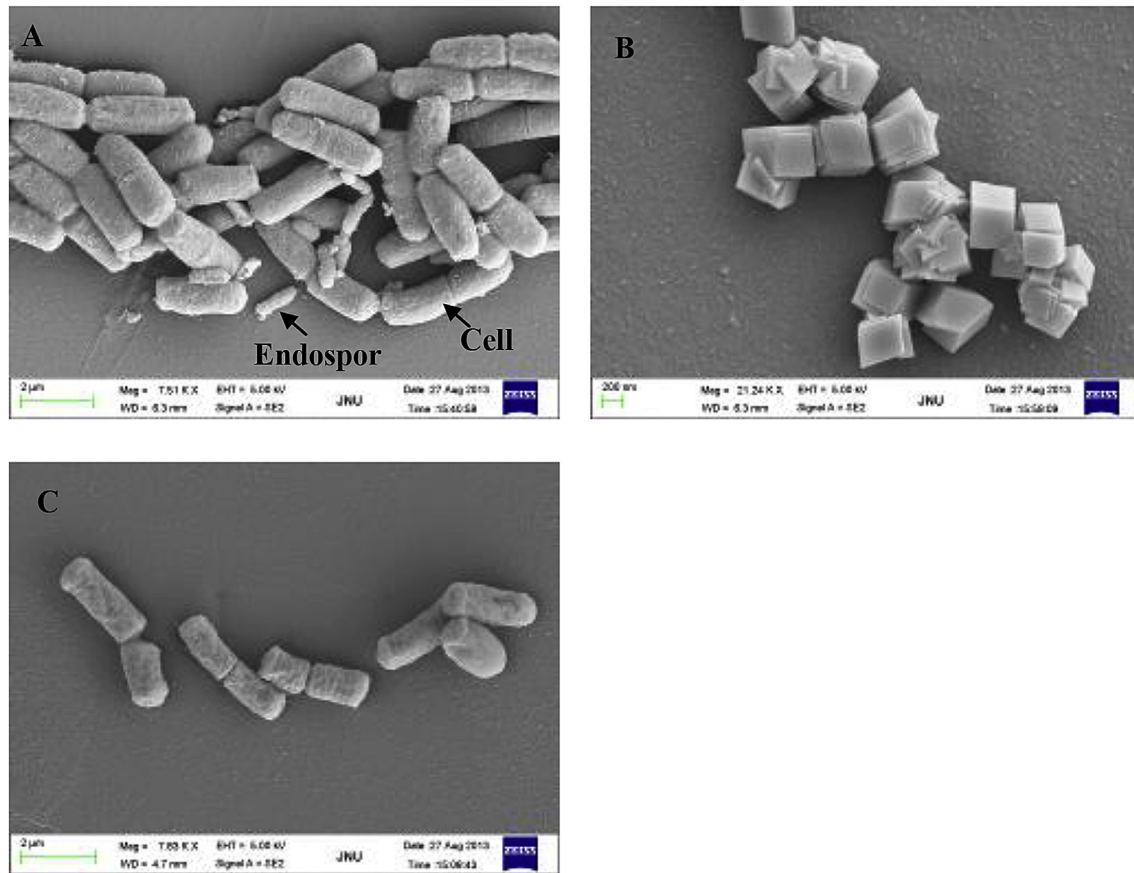


Fig. 4. Morphology of *B. thuringiensis*. (A) Morphology of *B. thuringiensis* and endospores after TPT degradation, (B) morphology of crystalline proteins after TPT degradation, and (C) morphology of *B. thuringiensis* before TPT degradation.

3.8. PT degradation pathway

To determine the dephenylation pathway, TPT, DPT and MPT at 1 mg L^{-1} were degraded separately. Fig. 6A demonstrates that TPT was transformed to DPT and MPT, of which DPT reached its maximal value of $233 \mu\text{g L}^{-1}$ at 0.5 d. An almost linear decline in DPT indicated that DPT was effectively degraded to MPT. The decreasing concentration of DPT over time accompanied with MPT accumulation at 2–4 d indicated that TPT dearylation occurred successively (Fig. 6). The concentration of DPT (Fig. 6) was higher than that of MPT during the entire degradation process. This established that MPT degradation was not the rate-limiting step.

4. Discussion

Trends similar to those of TPT degradation (Fig. 1A) were observed during dibutyltin biodegradation (Chen et al., 2016; Bernat et al., 2013). Both *Cochliobolus lunatus* and *Streptomyces* sp. transformed more than 90% of dibutyltin to monobutyltin on the initial day and degraded the residual dibutyltin during the following slow debutyltin period (Bernat et al., 2013). The slow degradation of TPT in the second phase was related to the decreasing concentration of residual TPT, which limited its sorption, transport and intracellular degradation. Moreover, without exogenous organic carbon, the metabolic activity of *B. thuringiensis* was negatively affected. The similar declining trends of residual dibutyltin and glucose during dibutyltin degradation also confirmed that exogenous nutrients played a crucial role in OT degradation. A decrease in these nutrients inhibit xenobiotic

transformation (Bernat et al., 2013). Furthermore, the increasing secretion of intracellular materials also inhibited bacterial metabolic activity, which in turn, depressed metabolism-dependent TPT degradation. From this study, it can be inferred that TPT removal initially involved sorption or accumulation and was gradually dominated by degradation. Additionally, the slow increase in TPT sorption or accumulation at 1–7 d was caused by a combination of TPT desorption and intracellular TPT efflux or the reduced binding of residual TPT to the cell surface.

TPT absorption by dead cells was independent of metabolism, primarily relying on TPT solubility, membrane permeability and the hydrophobic interaction of TPT with lipids and proteins that were the principal constituents of the membrane. However, sorption displayed a declining trend (Fig. 1B), illustrating that some absorbed TPT was desorbed. TPT desorbed by PBS washing was the fraction of TPT that bonded with the cellular surface by physical contact and not that entering the cytoplasm through active transport (Bonarska-Kujawa et al., 2012). The increasing TPT desorption (Fig. 1B) and decreasing TPT sorption at 3–7 d further confirmed this inference. Although degradation accounted for a large proportion of TPT removal (Huang et al., 2014), the removal by viable cells was still significantly lower than TPT sorption by dead cells in the first 2 days, suggesting that viable cells released some intracellular TPT (Ye et al., 2013a).

The results of the *in silico* modeling show that the distance between wall teichoic acids and TPT was less than 3.11 \AA , whereas the peptidoglycan mimic had a helical periodicity of 30 \AA and a 70 \AA pore in the middle of each hexagonal unit (Fig. 2). Therefore, TPT can be easily absorbed and transported into the cell wall. These

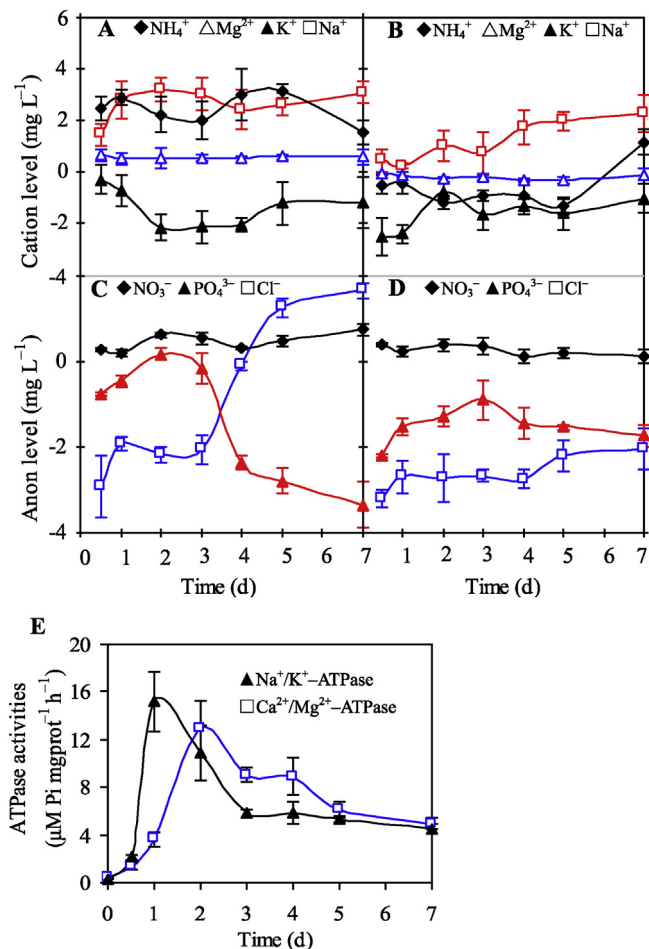


Fig. 5. Change in ion concentration. (A) Change in cation concentration during TPT degradation, (B) change in cation concentration without TPT, (C) change in anion concentration during TPT degradation, (D) change in anion concentration without TPT, and (E) change in Na⁺/K⁺-ATPase and Ca²⁺/Mg²⁺-ATPase activities during TPT degradation.

results were consistent with the declining trend in TPT sorption after 1 d (Fig. 1B). TPT removal was significantly higher than its degradation at 0.5 d and was followed by an increase in TPT degradation (Fig. 1A). This implied that initially TPT removal was largely due to sorption or accumulation and gradually dominated by degradation. The reduced contribution of sorption or accumulation to TPT removal at 1–7 d was caused by a combination of TPT desorption and intracellular TPT efflux or the decreased binding of residual TPT by the cell surface. Therefore, TPT removal by *B. thuringiensis* was the combined result of sorption, desorption, membrane transport, degradation, efflux and accumulation.

The increasing OD values (Fig. 3A) showed that the cell membrane changed with time. Therefore, ONPG could be transported into the cell, inducing β-galactosidase, which affected its hydrolysis (Shi et al., 2013). As membrane toxins, PTs could modify membrane hydration and alter some receptor proteins important for lipid metabolism (Higley et al., 2013), resulting in increased permeability. In contrast to DPT and MPT, trisubstituted TPT, which had the highest lipophilicity, induced the most significant membrane modifications, enlarging the gaps among the hydrophobic tails of phospholipids and forming holes in the membrane. These results confirmed that TPT increased membrane permeability. TPT desorption and release triggered by increased permeability partially explained the slow increase in sorption or accumulation

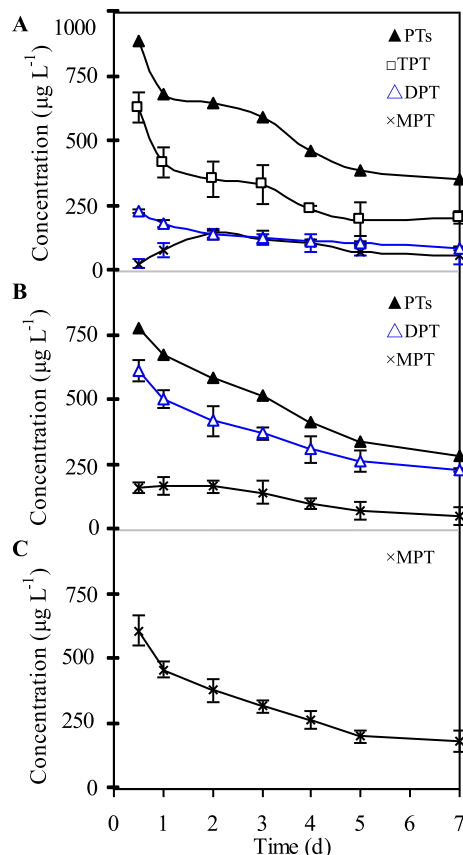


Fig. 6. PT degradation by 0.3 g L⁻¹ *B. thuringiensis* for 0.5–7 d. (A) TPT degradation and its metabolites, (B) DPT degradation and its metabolite, (C) MPT degradation.

(Fig. 1).

The ascending phases of arabinose and oxalic acid uptake were also consistent with the increase in membrane permeability, which further proved that TPT exerted a suppressive effect on the membrane, inducing the efflux of intracellular materials. The subsequent decline in the concentrations of arabinose and oxalic acid indicated that their assimilation predominated over secretion in this period (Fig. 3B). Oxalic acid released by yeast also exhibited an increasing trend during photocatalysis because of an increase in membrane permeability (Thabet et al., 2013). Barring arabinose, no other monosaccharides were detected in the current study, illustrating that the released materials were effectively absorbed or reused by the viable cells. The assimilation of these released materials maintained cellular metabolic activities, increasing TPT degradation efficiencies and cell viability as demonstrated in Figs. 1A and 3A.

TPT degradation was a metabolic process that was related to ion transport, which is primarily attributed to ion channel activation, membrane alteration, ion exchange, cell metabolism, or combinations of the above. Ion channels can be activated by various stimuli, including TPT stress. Na⁺ was an essential cation for energy metabolism and ion homeostasis. Its efflux is usually considered to indicate a change in membrane permeability (Buckel and Thauer, 2013). Similar to ion exchange during adsorbate binding (Ye et al., 2013b), Mg²⁺ and Na⁺ release (Fig. 5A) could balance the bio-sorption of PTs. TPT degraded inactive proteins, altered protein topological structures and inhibited protein synthesis (Graceli et al., 2013), resulting in a decrease in protein content (Fig. S3). NH₄⁺ is a common intracellular ion and a component of proteins. Its release is related to an increase in both membrane permeability and

protein degradation. NH_4^+ generated via protein and phospholipid photocatalysis was gradually released by yeast (Thabet et al., 2013). The accumulation of K^+ and PO_4^{3-} (Fig. 5) might be related to their cellular functions. K^+ is involved in various metabolic activities and is transported by Na^+/K^+ -ATPase in the opposite direction compared with Na^+ . PO_4^{3-} , an important anion for metabolism in all forms of life, takes part in various metabolic processes. Therefore, high-energy phosphate conversion could account for PO_4^{3-} transport in the present study. PO_4^{3-} uptake through cotransport with H^+ or Na^+ results in PO_4^{3-} accumulation against its gradient (Biber et al., 2013). The same direction of K^+ and PO_4^{3-} flux during PO_4^{3-} uptake by *Leishmania infantum* was consistent with the current findings (Russo-Abrahão et al., 2013). These findings clearly confirmed that TPT was responsible for the increased release of ions and other materials.

Membrane permeability as well as Cl^- and oxalic acid release exhibited significant correlations with time, which confirmed that TPT caused membrane alteration, increasing cellular material release (Table S2). Because Cl^- release was significantly correlated with most factors, namely, time, TPT degradation, removal, sorption, cell permeability and viability, it could be considered as an indicator of membrane permeability change during TPT treatment. However, most of the detected intracellular molecules, including NO_3^- , PO_4^{3-} , Na^+ , NH_4^+ , K^+ , Mg^{2+} and arabinose, were not significantly correlated with increasing membrane permeability. The above findings showed that either these released materials were effectively absorbed by cells or their transport was not affected by TPT and membrane alteration.

To further understand the ion transport process, related transport proteins were analyzed (Table S1). Na^+/K^+ - and $\text{Ca}^{2+}/\text{Mg}^{2+}$ -ATPases are two ATP-hydrolyzing enzymes that control ion gradients essential for signal transduction and active transport (Ogawa et al., 2015). Potassium-transporting ATPases (KdpA, KdpB and KdpC) are components of the high-affinity ATP-driven potassium transporters, which catalyze the hydrolysis of ATP coupled with the exchange of hydrogen and potassium ions (Castillo et al., 2015). The calcium transport ATPase YloB catalyzes ATP hydrolysis and mediates calcium transport. The phosphate ABC transporter permease YqgH is part of a binding-protein-dependent transporter, which is responsible for the translocation of substrates across the membrane. The initial rapid assimilation of PO_4^{3-} was caused by phosphorylation during TPT degradation. With the rapidly increasing degradation, ATP hydrolysis generated some PO_4^{3-} , reducing PO_4^{3-} assimilation, which was in agreement with the increasing trend for PO_4^{3-} up to 2 d (Fig. 5C). The slow increase in TPT degradation after 2 d reduced ATP hydrolysis and decreased PO_4^{3-} production, accounting for the increased assimilation of PO_4^{3-} . The energy generated by ATP hydrolysis acted as a driving force for the active transport of Na^+ and K^+ ions against their gradients. Na^+ efflux and K^+ assimilation shown in Fig. 5A revealed that Na^+/K^+ -ATPase influenced transport as this enzyme is a mediator that transports three intracellular Na^+ out of the cell and two extracellular K^+ into the cell (Monti et al., 2013). The similar exponential increase in the protease, esterase and amylase activities of *B. thuringiensis* from 12 to 42 h indicated that these enzymes were linked to pollutant degradation (Surhio et al., 2014).

Additionally, KtrA, KtrB, KtrC, KtrD, TrkA and TrkB are associated with K^+ uptake and release. Of these proteins, an octameric catalytic ring of KtrC and a membrane associated dimer of KtrD form a complex that functions as a channel for K^+ uptake (Gries et al., 2013; Price-Whelan et al., 2013). TrkA and TrkB are integral membrane proteins for K^+ transport, regulating ion transport either by direct binding or physicochemical properties (Anishkin et al., 2014). However, transporter activity (Vieira-Pires et al., 2013) required not just ATP but also a suitable stimulus to activate the intramembrane

gate in the current study (Fig. 5). The sodium ABC transporter permeases YhaP and NatB (Table S1) are involved in ATP-dependent electrogenic sodium extrusion (Lewinson and Livnat-Levanon, 2017; Neumann et al., 2017). Another transporter, the NH_4^+ transporter protein (AmtB), is responsible for the transport of various substrates across membranes (Laganowsky et al., 2014; Weiner and Verlander, 2011), which might be associated with Mg^{2+} , NH_4^+ and NO_3^- efflux (Fig. 5). As for the proteins MgtA, MgtC and MgtE, these acted as magnesium transporters that were responsible for Mg^{2+} balance (Cromie and Groisman, 2010; Shin et al., 2014). Nitrite extrusion permease (NarK) is involved in the excretion of nitrite produced by the dissimilatory reduction of nitrate (Yan et al., 2013; Zheng et al., 2013). The synthesis of these transporters confirmed substrate transport during the TPT biodegradation process.

As for the TPT biodegradation pathway, successive dearylation was recognized as the main pathway through environmental monitoring and TPT degradation experiments, whereas direct TPT degradation to MPT has also been found (Antes et al., 2011; Ye et al., 2013a). The molecular properties of TPT were calculated (Table S3), which showed that Sn-C bonds of TPT had the lowest energy, and therefore, they were the most easily hydrolyzed bonds. Because of the asymmetric topology of TPT, these three covalent bonds connecting benzene and tin have unequal bond energies, which were 0.0034, 0.0059 and 0.0072 kcal mol⁻¹ Å (Table S3), respectively. These results indicated that the cleavage reactions of the Sn-C bonds of TPT occurred successively. Further degradation of the produced DPT and MPT (Fig. 6) was correlated with a slow increase in TPT degradation efficiency over time.

5. Conclusions

TPT at 1 mg L⁻¹ was successively transformed to DPT and MPT by 0.3 g L⁻¹ of *B. thuringiensis* with a degradation efficiency of up to 78.2% in 7 d. During this process, some intracellular arabinose, oxalic acid, Na^+ , NH_4^+ , Mg^{2+} , NO_3^- , endospores and crystalline proteins were released because of the increased membrane permeability and activities of transport proteins. The increased assimilation of K^+ and PO_4^{3-} and reuse of some released materials by viable cells through the involvement of Na^+/K^+ - and $\text{Ca}^{2+}/\text{Mg}^{2+}$ -ATPases improved cellular viability as well as increased PT sorption and degradation. These findings, obtained by an analysis of cellular metabolic responses, provide insights into TPT transport and degradation mechanisms.

Acknowledgements

The authors would like to thank the National Natural Science Foundation of China (Nos. 21577049, 21377047), Science and Technology Project of Guangdong Province (Nos. 2014A020216013, 2016A020222005) and Science and Technology Project of Guangzhou City (No. 201707010255) for their financial support.

Appendix A. Supplementary data

Supplementary data related to this article can be found at <http://dx.doi.org/10.1016/j.ibiod.2017.04.020>.

References

- Adams, W.A., Xu, Y., Little, J.C., Fristachi, A.F., Rice, G.E., Impellitteri, C.A., 2011. Predicting the migration rate of dialkyl organotins from PVC pipe into water. *Environ. Sci. Technol.* 45, 6902–6907.
- Anishkin, A., Loukin, S.H., Teng, J., Kung, C., 2014. Feeling the hidden mechanical forces in lipid bilayer is an original sense. *Proc. Natl. Acad. Sci. U. S. A.* 111, 7898–7905.

- Antes, F.G., Krupp, E., Flores, E.M.M., Dressler, V.L., Feldmann, J., 2011. Speciation and degradation of triphenyltin in typical paddy fields and its uptake into rice plants. *Environ. Sci. Technol.* 45, 10524–10530.
- Bernat, P., Szweczyk, R., Krupiński, M., Długosiński, J., 2013. Butyltins degradation by *Cunninghamella elegans* and *Cochliobolus lunatus* co-culture. *J. Hazard. Mater.* 246, 277–282.
- Biber, J., Hernandez, N., Forster, I., 2013. Phosphate transporters and their function. *Annu. Rev. Physiol.* 75, 535–550.
- Bonarska-Kujawa, D., Kleszczyńska, H., Przesalski, S., 2012. The location of organotins within the erythrocyte membrane in relation to their toxicity. *Ecotox. Environ. Safe* 78, 232–238.
- Buckel, W., Thauer, R.K., 2013. Energy conservation via electron bifurcating ferredoxin reduction and proton/Na⁺ translocating ferredoxin oxidation. *Biochim. Biophys. Acta* 1827, 94–113.
- Castillo, J.P., Rui, H., Basilio, D., Das, A., Roux, B., Latorre, R., Bezanilla, F., Holmgren, M., 2015. Mechanism of potassium ion uptake by the Na⁺/K⁺-ATPase. *Nat. Commun.* 6, 7622.
- Chen, C.W., Chen, C.F., Ju, Y.R., Dong, C.D., 2016. Assessment of the bioaccumulation and biodegradation of butyltin compounds by *Thalassia crenata* in Kaohsiung Harbor, Taiwan. *Int. Biodeterior. Biodegr.* 113, 97–106.
- Cromie, M.J., Groisman, E.A., 2010. Promoter and riboswitch control of the Mg²⁺ transporter *mgtA* from *Salmonella enterica*. *J. Bacteriol.* 192, 604–607.
- Deleu, M., Crowet, J.M., Nasir, M.N., Lins, L., 2014. Complementary biophysical tools to investigate lipid specificity in the interaction between bioactive molecules and the plasma membrane: a review. *Biochim. Biophys. Acta* 1838, 3171–3190.
- Fortibuoni, T., Noventa, S., Rampazzo, F., Gion, C., Formalewicz, M., Berto, D., Raicevich, S., 2013. Evidence of butyltin biomagnification along the Northern Adriatic food-web (Mediterranean Sea) elucidated by stable isotope ratios. *Environ. Sci. Technol.* 47, 3370–3377.
- Gao, J., Ye, J.S., Ma, J.W., Tang, L.T., Huang, J., 2014. Biosorption and biodegradation of triphenyltin by *Stenotrophomonas maltophilia* and their influence on cellular metabolism. *J. Hazard. Mater.* 276, 112–119.
- Graceli, J.B., Sena, G.C., Lopes, P.F.I., Zamprogno, G.C., Costa, M.B.D., Godoi, A.F.L., Santos, D.M.D., Marchi, M.R.R.D., Fernandez, M.A.D.S., 2013. Organotins: a review of their reproductive toxicity, biochemistry, and environmental fate. *Reprod. Toxicol.* 36, 40–52.
- Gries, C.M., Bose, J.L., Nuxoll, A.S., Fey, P.D., Bayles, K.W., 2013. The Ktr potassium transport system in *Staphylococcus aureus* and its role in cell physiology, antimicrobial resistance and pathogenesis. *Mol. Microbiol.* 89, 760–773.
- Higley, E., Tompsett, A.R., Giesy, J.P., Hecker, M., Wiseman, S., 2013. Effects of triphenyltin on growth and development of the wood frog (*Lithobates sylvaticus*). *Aquat. Toxicol.* 144, 155–161.
- Huang, J., Ye, J.S., Ma, J.W., Gao, J., Chen, S.Q., Wu, X.L., 2014. Triphenyltin biosorption, dephenylation pathway and cellular responses during triphenyltin biodegradation by *Bacillus thuringiensis* and tea saponin. *Chem. Eng. J.* 249, 167–173.
- Laganowsky, A., Reading, E., Allison, T.M., Ulmschneider, M.B., Degiacomi, M.T., Baldwin, A.J., Robinson, C.V., 2014. Membrane proteins bind lipids selectively to modulate their structure and function. *Nature* 510, 172–175.
- Lewinson, O., Livnat-Levanon, N., 2017. Mechanism of action of ABC importers: conservation, divergence, and physiological adaptations. *J. Mol. Biol.* 429, 606–619.
- Lu, J., Feng, J.H., Cai, S.H., Chen, Z., 2017. Metabolomic responses of *Halotilus diversicolor* to organotin compounds. *Chemosphere* 168, 860–869.
- Mandal, K., Singh, B., Jariyal, M., Gupta, V.K., 2013. Microbial degradation of fipronil by *Bacillus thuringiensis*. *Ecotox. Environ. Safe* 93, 87–92.
- Mathurasa, L., Tongcumpou, C., Sabatini, D., Luepromchai, E., 2012. Anionic surfactant enhanced bacterial degradation of tributyltin in soil. *Int. Biodeterior. Biodegr.* 75, 7–14.
- Monti, J.L.E., Montes, M.R., Rossi, R.C., 2013. Alternative cycling modes of the Na⁺/K⁺-ATPase in the presence of either Na⁺ or Rb⁺. *Biochim. Biophys. Acta* 1828, 1374–1383.
- Neumann, J., Rose-Sperling, D., Hellmich, U.A., 2017. Diverse relations between ABC transporters and lipids: an overview. *Biochim. Biophys. Acta* 1859, 605–618.
- Ogawa, H., Cornelius, F., Hirata, A., Toyoshima, C., 2015. Sequential substitution of K⁺ bound to Na⁺, K⁺-ATPase visualized by X-ray crystallography. *Nat. Commun.* 6, 8004.
- Oliveira, R.D., Santelli, R.E., 2010. Occurrence and chemical speciation analysis of organotin compounds in the environment: a review. *Talanta* 82, 9–24.
- Price-Whelan, A., Poon, C.K., Benson, M.A., Eidem, T.T., Roux, C.M., Boyd, J.M., Dunman, P.M., Torres, V.J., Krulwich, T.A., 2013. Transcriptional profiling of *Staphylococcus aureus* during growth in 2 M NaCl leads to clarification of physiological roles for Kdp and Ktr K⁺ uptake systems. *mBio* 4, e00407–13.
- Renzi, M.T., Amichot, M., Pauron, D., Tchamitchian, S., Brunet, J.L., Kretschmar, A., Maimi, S., Belzunces, L.P., 2016. Chronic toxicity and physiological changes induced in the honey bee by the exposure to fipronil and *Bacillus thuringiensis* spores alone or combined. *Ecotox. Environ. Safe* 127, 205–213.
- Russo-Abrahão, T., Alves-Bezerra, M., Majerowicz, D., Freitas-Mesquita, A.L., Dick, C.F., Gondim, K.C., Meyer-Fernandes, J.R., 2013. Transport of inorganic phosphate in *Leishmania infantum* and compensatory regulation at low inorganic phosphate concentration. *Biochim. Biophys. Acta* 1830, 2683–2689.
- Schmidt, A., Haferburg, G., Schmidt, A., Lischke, U., Merten, D., Ghergel, F., Büchel, G., Kothe, E., 2009. Heavy metal resistance to the extreme: *Streptomyces* strains from a former uranium mining area. *Chem. Erde-Geochem* 69, 35–44.
- Shi, G.Y., Yin, H., Ye, J.S., Peng, H., Li, J., Luo, C.L., 2013. Effect of cadmium ion on biodegradation of decabromodiphenyl ether (BDE-209) by *Pseudomonas aeruginosa*. *J. Hazard. Mater.* 263, 711–717.
- Shin, J.H., Wakeman, C.A., Goodson, J.R., Rodionov, D.A., Freedman, B.G., Senger, R.S., Winkler, W.C., 2014. Transport of magnesium by a bacterial *nramp*-related gene. *PLoS Genet.* 10, e1004429.
- Surhio, M.A., Talpur, F.N., Nizamani, S.M., Amin, F., Bong, C.W., Lee, C.W., Ashraf, M.A., Shah, M.R., 2014. Complete degradation of dimethyl phthalate by biochemical cooperation of the *Bacillus thuringiensis* strain isolated from cotton field soil. *RSC Adv.* 4, 55960–55966.
- Takabe, Y., Kameda, I., Suzuki, R., Nishimura, F., Itoh, S., 2014. Changes of microbial substrate metabolic patterns through a wastewater reuse process, including WWTP and SAT concerning depth. *Water Res.* 60, 105–117.
- Tang, L.T., Wang, L.L., Ou, H.S., Li, Q.S., Ye, J.S., Yin, H., 2016. Correlation among phenyltins molecular properties, degradation and cellular influences on *Bacillus thuringiensis* in the presence of biosurfactant. *Biochem. Eng. J.* 105, 71–79.
- Thabet, S., Weiss-Gayet, M., Dappozze, F., Cotton, P., Guillard, C., 2013. Photocatalysis on yeast cells: toward targets and mechanisms. *Appl. Catal. B* 140, 169–178.
- Vieira-Pires, R.S., Szollosi, A., Morais-Cabral, J.H., 2013. The structure of the KtrAB potassium transporter. *Nature* 496, 323–328.
- Wang, X.B., Chen, J.W., Wang, Y., Xie, H.B., Fu, Z.Q., 2015. Transformation pathways of MeO-PBDEs catalyzed by active center of P450 enzymes: a DFT investigation employing 6-MeO-BDE-47 as a case. *Chemosphere* 120, 631–636.
- Weiner, I.D., Verlander, J.W., 2011. Role of NH₃ and NH₄⁺ transporters in renal acid-base transport. *Am. J. Physiol. Ren. Physiol.* 300, F11–F23.
- Yan, H.C., Huang, W.Y., Yan, C.Y., Gong, X.Q., Jiang, S.R., Zhao, Y., Wang, J.W., Shi, Y.G., 2013. Structure and mechanism of a nitrate transporter. *Cell Rep.* 3, 716–723.
- Ye, J.S., Yin, H., Peng, H., Bai, J.Q., Xie, D.P., Wang, L.L., 2013a. Biosorption and biodegradation of triphenyltin by *Brevibacillus brevis*. *Bioresour. Technol.* 129, 236–241.
- Ye, J.S., Yin, H., Xie, D.P., Peng, H., Huang, J., Liang, W.Y., 2013b. Copper biosorption and ions release by *Stenotrophomonas maltophilia* in the presence of benzo[a]pyrene. *Chem. Eng. J.* 219, 1–9.
- Yi, A.X., Leung, K.M.Y., Lam, M.H.W., Lee, J.S., Giesy, J.P., 2012. Review of measured concentrations of triphenyltin compounds in marine ecosystems and meta-analysis of their risks to humans and the environment. *Chemosphere* 89, 1015–1025.
- Zhao, Y.J., He, J.C., Chen, Q., He, J., Hou, H.Q., Zheng, Z., 2011. Evaluation of 206 nm UV radiation for degrading organometallics in wastewater. *Chem. Eng. J.* 167, 22–27.
- Zheng, H., Wisedchaisri, G., Gonen, T., 2013. Crystal structure of a nitrate/nitrite exchanger. *Nature* 497, 647–651.